JACS
JOURNAL OF THE AMERICAN CHEMICAL SOCIETY
Article
pubs.acs.org/JACS

Dual Element Intercalation into 2D Layered Bi_2Se_3 Nanoribbons

Karen P. Chen, Frank R. Chung, Mengjing Wang, and Kristie J. Koski*

Department of Chemistry, Brown University, 324 Brook St. Box H, Providence Rhode Island 02912, United States

Supporting Information

ABSTRACT: We demonstrate the intercalation of multiple zero-valent atomic species into two-dimensional (2D) layered Bi_2Se_3 nanoribbons. Intercalation is performed chemically through a stepwise combination of disproportionation redox reactions, hydrazine reduction, or carbonyl decomposition. Traditional intercalation is electrochemical thus limiting intercalant guests to a single atomic species. We show that multiple zero-valent atoms can be intercalated through this chemical route into the host lattice of a 2D crystal. Intermetallic species exhibit unique structural ordering demonstrated in a variety of superlattice diffraction patterns. We believe this method is general and can be used to achieve a wide variety of new 2D materials previously inaccessible.

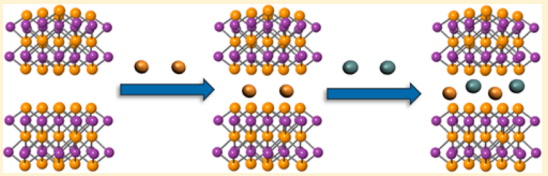

1. INTRODUCTION

Intercalation is the critical ingredient to a multitude of energy storage technologies ranging from batteries to supercapacitors and is a powerful method for modifying a material's properties, structure, and behavior.[1−3] Most intercalation techniques are electrochemical, relying on intercalants' ionic charge to move them into and out of materials. However, electrochemical methods have proven practically incapable of intercalating more than one chemical species, despite much effort.[4−9] Dual intercalation remains a long-standing goal in battery research because of its potential to increase energy storage and to enable alternative technologies such as rocking chair batteries.[7−9] Further, multispecies intercalation is desirable for much the same reason alloying is desirable in materials science: It can provide access to an enormous new range of material structures with properties unattainable with a single species.

Recently, it has been shown that it is possible to intercalate high densities of zero-valent metal, such as Cu, Co, Sn, etc., into a variety of layered and two-dimensional (2D) materials.[10−12] Intercalated metals form unique structures within the host and have unusual properties specific to a confined, isolated atomically thin metal. Thus far, only one atomic species at a time has been intercalated. In this work, we present a chemical route for the intercalation of multiple zero-valent atomic species into the van der Waals gaps of layer-structured Bi_2Se_3 nanoribbons. Bi_2Se_3 is a topological insulator and thermoelectric material that has recently attracted enormous interest.[13,14] It is fairly robust to processing, hosting extremely high densities of zero-valent metal atoms such as copper and cobalt (e.g., up to 60 at % Cu and 30 at % Co).[10,11] The multiple element intercalation process relies on a stepwise combination of disproportionation redox reactions, hydrazine reduction, or carbonyl decomposition of precursors to essentially form an interlayer, 2D alloy inside the host lattice. Through intercalating multiple zero-valent metals, these layered materials can be transformed to metastable states with unique properties. This synthetic technique may serve as a method to precisely modulate desired mechanical, optical, and electronic properties. Further, as evidenced by demonstration with 30 different ordered pairs of elements, we expect that this method is general[12] and can be used to form many different 2D alloys in a variety of layered materials.

2. EXPERIMENTAL SECTION

Bi_2Se_3 nanoribbons were grown using the vapor−liquid−solid (VLS) technique.[14] Quartz substrates were used for growth along with 20 nm gold colloid as a catalyst. Nanoribbons are approximately 1−10 μm in length and 1 μm in width and, on average, 100 nm in thickness. Zero-valent metals were individually intercalated using the methods of Koski et al.[10,11] Metals were intercalated consecutively into the nanoribbons on the growth substrate to form intercalated alloys. Before each intercalation, all glassware was allowed to sit overnight in slightly acidic distilled water (4.0−6.5 pH) and then dried in an oven for 24 h. Between multiple intercalations, the nanoribbons on the substrates were rinsed thoroughly with acetone and air-dried for at least 10 min. The reaction scheme is shown in Scheme 1.

A disproportionation redox reaction was used to intercalate Cu and Sn. Bi_2Se_3 nanoribbons on a quartz substrate were placed under reflux

Scheme 1. Intercalation of Multiple Zero-Valent Metal Atoms into Bi_2Se_3

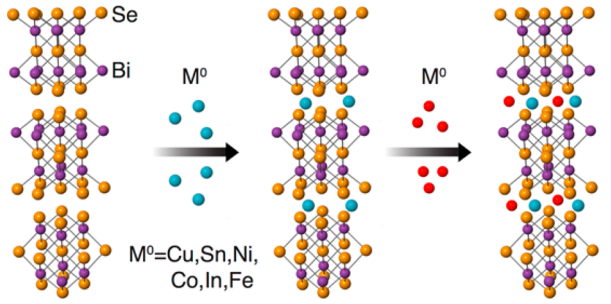

Received: January 20, 2015
Published: April 8, 2015

DOI: 10.1021/jacs.5b00666
J. Am. Chem. Soc. 2015, 137, 5431−5437

in a solution of roughly 1 mg of the specific precursor and 5 mL of acetone at about 45 °C for 30−60 min. The precursors are tetrakis (acetonitrile) copper(I) hexafluorophosphate and stannous chloride with 0.1 g tartaric acid, for Cu and Sn, respectively. Nanoribbons were rinsed with hot acetone, ∼35 °C, and air-dried. We found that if Cu is the second intercalant, it is possible to completely remove the previous intercalant simply by performing the disproportionation redox reaction of Cu(I) for an extended period of time.

To intercalate Ni, a substrate containing Bi_2Se_3 nanoribbons was placed into a 20 mL vial with a solution of 1 mg of nickel(II) nitrate pentahydrate and 5 mL of acetone. Slowly, 1 mL of hydrazine hydrate was added dropwise to the vial reducing Ni(II) to yield Ni(0) in a highly exothermic reaction. The solution changed from a light blue-green to lavender and then turned clear. After sitting for about 10 min, the substrate was taken out, rinsed with hot acetone, and air-dried.

To intercalate Co and Fe, we performed a carbonyl decomposition reaction under inert atmosphere in solution. A substrate with Bi_2Se_3 nanoribbons was placed in a round-bottom flask, evacuated, and flushed with N_2 gas. 5 mL of air-free acetone was added to the flask and heated to reflux (about 45 °C). About 0.5 mg of dicobalt octacarbonyl or 1 mg of iron pentacarbonyl in 3 mL of air-free acetone was added dropwise to the flask over 1 h. Substrates were then removed, rinsed with hot acetone, and air-dried. We found that it is very difficult to intercalate iron because it does not disproportionate easily at lower temperatures, but with another intercalant already in the crystal, higher concentrations of Fe are achievable, reaching as high as 21.4 at %, while the most we could achieve with a single Fe intercalation was 7.5 at %.

To intercalate In, we used a disproportionation reaction under inert atmosphere in solution. Bi_2Se_3 nanoribbons on a quartz substrate were placed in a three-neck flask, evacuated, and flushed with N_2 gas. Five mL of air-free acetone was heated to reflux (about 55 °C), and then 1 mg of InCl in 3 mL of acetone was added dropwise over 1 h. The substrate was removed, washed with hot acetone, and air-dried.

The concentration of the first intercalant can be controlled through reaction time or initial reactant concentration.[10,11] The total final intercalant concentration of the two species, however, has no obvious dependence on either precursor concentration or reaction time (Supporting Information). Intercalated samples are stored in a glovebox under inert atmosphere for their entire lifetime (∼3−4 months). Oxidation of the Bi_2Se_3 host slowly occurs over this time period destroying intercalant ordering and nanoribbon morphology.[15]

Transmission electron microscopy (TEM) images, selected area electron diffraction (SAED), and energy dispersive X-ray spectra (EDX) were collected with a JEOL 2100F operating at 200 keV. X-ray diffraction data were acquired with a copper source (Cu Kα1 = 1.5406 Å, Kα2 =1.54439 Å) from a Bruker D8 Discover diffractometer. Lattice parameters were determined using a Rietveld Refinement with Maud.[16] SEM images were collected using a LEO 1530 VP scanning electron microscope (SEM) with energy-dispersive X-ray spectroscopy (EDX). Raman scattering measurements were collected with a WiTec micro-Raman spectrometer using a Nd:YAG laser (λ = 532 nm; <5 mW) as excitation. Scattering was collected using a 100× objective with an 1800 g/mm grating and an edge filter with a cutoff of ∼50 cm^{-1}.

3. RESULTS AND DISCUSSION

Bi_2Se_3 is a layered chalcogenide material (Scheme 1). It has a rhombohedral crystal structure (space group: D_{3d}^5 ($R\bar{3}m$)). Each covalently bonded layer of Bi_2Se_3 is denoted a quintuple layer as it contains five atomic layers, alternating as Se−Bi−Se−Bi-Se.

Elemental Composition. The elemental composition of each set of intercalated nanoribbons is characterized using TEM-EDX spectroscopy on an average of 3−5 nanoribbons (Figure 1a,b). Figure 1a shows a STEM-EDX line scan across a single nanoribbon intercalated with iron (2.8 at %) and cobalt (15.7 at %). Cobalt and iron are distributed homogeneously

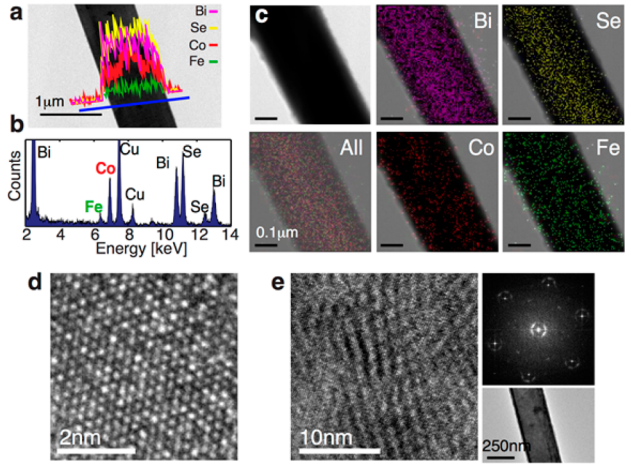

Figure 1. (a) STEM-EDX linescan of Bi_2Se_3 nanoribbons intercalated with 2.8 at % Fe and 15.7 at % Co showing distribution of iron and cobalt throughout the ribbon. (b) EDX spectrum of the nanoribbon and (c) STEM-EDX map of another Fe/Co-intercalated Bi_2Se_3 nanoribbon showing Co and Fe throughout. (d) High-resolution TEM image of Fe/Cu intercalated nanoribbon and (e) high-resolution TEM image of In/Co-intercalated Bi_2Se_3 nanoribbon showing the stripe-phase of an incommensurate charge density wave also revealed in the Fourier transform of the image (upper right inset), while at lower magnification the ribbon shows nearly uniform contrast (lower right inset).

throughout the nanoribbon and show no aggregation within the host. An EDX spectrum of the entire nanoribbon (Figure 1b) shows the Fe and Co signal; Cu TEM grids are used to eliminate overlap in the elemental characterization. A STEM-EDX map (Figure 1c) of another Bi_2Se_3 nanoribbon intercalated with iron and cobalt shows that the iron and cobalt are also distributed evenly throughout the nanoribbon. The poor signal-to-background ratio of the iron signal accounts for some spurious counts outside of the ribbon. Similar measurements on Cu/Fe, In/Ni, and Fe,Co-intercalated nanoribbons are presented in Supporting Information, along with example EDX spectra of all nanoribbons measured here. Homogeneous distribution of the zero-valent intercalants with no evidence of aggregated islands within the host is found for all nanoribbons. High-resolution images (Figure 1d,e) show that intercalated nanoribbons maintain a high crystal quality after processing. Figure 1e shows the stripe phase of an incommensurate charge density wave in nanoribbons intercalated with In/Co along with the Fourier transform of the high-resolution image. This pattern is similar to other layered material systems that show a Bragg signature of a charge density waves, including those found in Bi_2Se_3 nanoribbons intercalated with only one atomic species.[11,17]

Superlattice Electron Diffraction Patterns. One of the key signatures of intercalation is the formation of a superlattice pattern that can be observed using TEM electron diffraction.[1,3] These patterns indicate the degree and type of order and disorder of the intercalants as well as, in some cases, charge density waves and periodic distortions of the host lattice. Figure 2 presents a chart of the resulting superlattice patterns formed through 30 different cases of zero-valent intercalation of two different metals, with rows representing the first intercalated elements and columns representing the second.

Each pattern falls into one or more of six categories, described below, as represented by colored outlines in Figure 2.

DOI: 10.1021/jacs.5b00666
J. Am. Chem. Soc. 2015, 137, 5431−5437

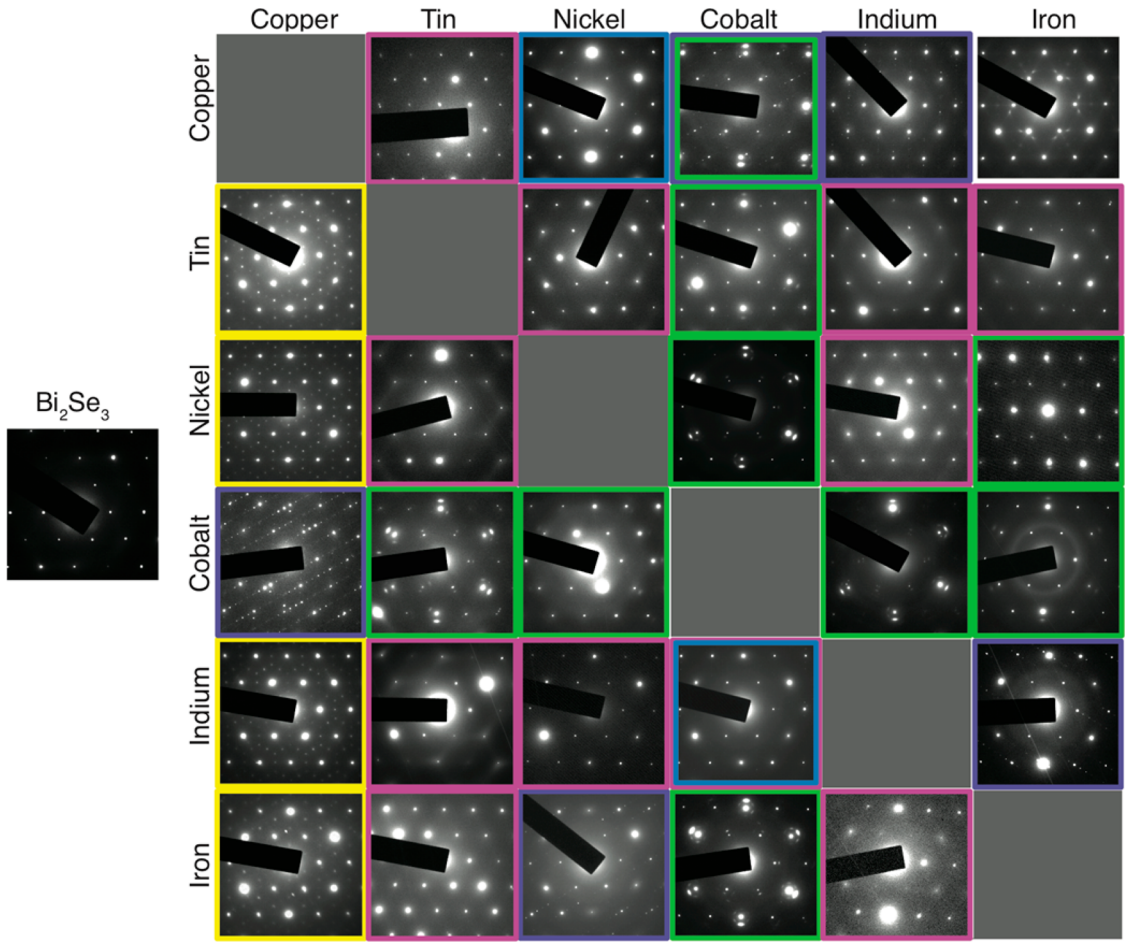

Figure 2. Superlattice diffraction patterns of dual metals intercalated into Bi_2Se_3 nanoribbons. Outlined colors identify categories of superlattice ordering. Rows are first intercalants; columns are second. Further details can be found in the manuscript.

Table 1. Lattice Constants of Dual Zero-Valent Metal-Intercalated Bi_2Se_3 Nanoribbons

intercalant	composition (at %)		$a \pm 0.001$ Å	$c \pm 0.003$ Å	intercalant	composition		$a \pm 0.001$ Å	$c \pm 0.003$ Å
none			4.136	28.53					
Cu/Sn	4.5 ± 1.0	3.0 ± 3.0	4.129	28.62	In/Ni	4.0 ± 1.6	0.3 ± 0.3	4.141	28.75
Cu/Co	1.4 ± 2.5	3.5 ± 0.9	4.139	28.58	In/Cu	0.7 ± 0.2	44.9 ± 1.4	4.160	28.83
Cu/In	2.7 ± 2.3	5.4 ± 0.5	4.138	28.61	In/Sn	0.3 ± 0.3	1.4 ± 1.4	4.167	28.68
Cu/Fe	7.0 ± 6.5	11 ± 10.0	4.151	28.74	In/Co	1.8 ± 0.5	0.2 ± 0.2	4.150	28.68
Cu/Ni	3.5 ± 2.5	3.5 ± 1.0	4.154	28.73	In/Fe	7.2 ± 1.0	4.2 ± 1.0	4.155	28.71
Co/Cu	0.2 ± 0.3	39.8 ± 15	4.151	28.63	Ni/Sn	0.1 ± 0.1	0.3 ± 0.4	4.146	28.70
Co/Sn	3.8 ± 1.7	0.1 ± 0.1	4.149	28.27	Ni/Co	0.1 ± 0.2	25.3 ± 6.1	4.148	28.70
Co/Ni	15.3 ± 8.7	5.3 ± 4.1	4.154	28.73	Ni/In	0.1 ± 0.1	7.7 ± 4.0	4.138	28.73
Co/In	17.8 ± 3.0	1.7 ± 1.3	4.151	28.76	Ni/Cu	0.1 ± 0.1	0.7 ± 0.3	4.156	28.78
Co/Fe	6.7 ± 1.0	3.9 ± 0.2	4.168	28.67	Ni/Fe	0.2 ± 0.2	21.4 ± 9.2	4.160	28.68
Fe/Ni	8.9 ± 5.7	2.9 ± 2.9	4.142	28.77	Sn/Ni	1.5 ± 0.9	1.5 ± 1.1	4.145	28.65
Fe/Co	2.8 ± 0.1	15.7 ± 2.1	4.148	28.77	Sn/Co	0.3 ± 0.3	2.9 ± 1.4	4.147	28.70
Fe/Cu	3.3 ± 1.0	37.5 ± 10	4.175	28.70	Sn/In	2.5 ± 1.1	7.2 ± 6.1	4.147	28.78
Fe/Sn	1.0 ± 0.6	0.3 ± 0.5	4.173	28.70	Sn/Cu	0.3 ± 0.3	47 ± 7.6	4.154	28.55
Fe/In	5.3 ± 1.0	7.6 ± 1.0	4.153	28.67	Sn/Fe	1.4 ± 0.7	4.5 ± 0.9	4.175	28.77

All of these structures arose at room temperature, without thermal annealing. This is striking, because (with the exception[10] of Cu) single-element intercalation very rarely produces a superlattice pattern without heating to induce a disorder−order phase transition of the intercalant.[11] Even after annealing, strong superlattice diffraction patterns were observed previously only in Co, Cu, and Sn-intercalated Bi_2Se_3 nanoribbons. Yet we find that many different superlattices form readily at room temperature in the case of multiple intercalation, which suggests that the presence of two different atomic species creates a thermodynamic driving force favoring ordered 2D structures, perhaps analogous to well-known 3D intermetallic ordered structures such as B2.[18] Interestingly, many of the patterns in Figure 2 resemble the patterns produced by one or both of the single elements, in some cases suggesting a competition between two or more structures

DOI: 10.1021/jacs.5b00666
J. Am. Chem. Soc. 2015, 137, 5431−5437

resulting in an entirely new structure. Further, the dependence of structure on the order of intercalation suggests that at least some of these structures are metastable. The diffraction patterns are complex, and the degrees of freedom in the superlattice cells are many (especially for the disordered structures), so it is unlikely that the atomic structures can be confidently determined from these zone-axis patterns. Determination of all of these structures, and identification of the kinetic and thermodynamic variables that govern them, not only represents an enormous challenge but also a unique opportunity to explore the vast structural possibilities of 2D materials over the coming years.

Pink: Diffraction patterns outlined in pink are close to the original unintercalated Bi_2Se_3 diffraction pattern but contain streaking, very faint in some cases, aligned with the crystallographic axes. Such streaking indicates a statistical superposition of structures, i.e., disorder, associated with the zero-valent alloy intercalant. This may be the result of low intercalant concentration (see Table 1) or simply a result of the intercalant lacking order after room-temperature chemical processing. Note that all of these patterns contain either In or Sn, both low-melting-point p-block metals very different from the transition metals Fe, Co, Ni, and Cu.

Yellow: Diffraction patterns outlined with yellow show a superlattice pattern similar to a 2 × 2 × 1 pattern observed previously with intercalation of copper,[10] including families of spots such as {1−100} that are normally forbidden by the stacking symmetry in the rhombohedral Bi_2Se_3 host lattice (normally the lowest-order bright spots that appear are {11−20}) along with half-integer spots such as {11−20}/2. This pattern is consistent with a periodic array of groups of six copper atoms arranged in hexagons within the van der Waals gap. This pattern is observed in almost every case in which copper is intercalated as the second element, indicating a strong tendency of Cu to impose its own natural 2D superlattice structure almost without regard to the other intercalant. The exception is Co−Cu, which stands out with a uniquely strong 1D superlattice (purple). Yet even this pattern has many superlattice spots at the same or almost the same positions as the spots in the 2 × 2 × 1 Cu pattern. What makes this exception even more surprising is that very nearly all of the Co was displaced from the ribbon during the Cu intercalation (Table 1). With long intercalation times of the second copper intercalant, the first intercalant metal can be entirely displaced from the Bi_2Se_3 host, leaving Cu at concentrations as high as 60 at %.

Purple: Diffraction patterns outlined with purple show a 1D superlattice, with satellite spots displaced from the main Bragg spots along only one axis. Co−Cu stands out, in particular, with its extraordinarily strong 1D superlattice appearing at multiple diffraction orders, indicating a very coherent structure. We strongly suspect that the extremely strong superlattice pattern in the case of Co−Cu is due to competition from strong superlattice structures of Co and Cu. It may be two structures coexisting, perhaps with a unique stacking sequence in the third dimension. Cu−Co also includes a 1D superlattice, but it is not a dominant feature in the pattern in this case.

Green: Patterns outlined with green show a strained epitaxial-like pattern (i.e., the appearance of two diffraction patterns superposed and aligned, both with six-fold symmetry but with different lattice constants) very often associated with enhanced intensity of {3−300} higher-order Bragg spots relative to spots at lower order spots such as {11−20}. While the spots look similar to satellite spots commonly associated with incommensurate charge density waves in this class of materials,[3,11,17] the overall symmetry of the pattern, with each satellite at the same angular coordinate as its nearby Bragg spot, suggests that something else may be responsible. Single atomic intercalants of Co and Ag result in satellite spots that entirely surround the central Bragg spot in a circular pattern.[11] This pattern is strongly correlated with the presence of cobalt.

Blue: Diffraction patterns outlined with blue show higher order bright spots such as {3−300} bright spots with stronger intensities than the lower-order spots such as {11−20}. Changes of Bragg spot intensities typically indicate rearrangements within the original unit cell, possibly with a reduction of symmetry.

White: The pattern yielded by Cu/Fe intercalation defies categorization. While there are streaks, the streaks have strong intensity modulations with strong yet diffuse local peaks indicative of a disordered structure with a moderately well-defined (and likely incommensurate) superlattice periodicity. This diffraction pattern is likely the result of competing ordering of the copper and iron within the Bi_2Se_3 host.

In summary, superlattice structures can be controlled within the Bi_2Se_3 host lattice and are governed by a few key rules. If copper is intercalated second, this yields a 2 × 2 × 1 superlattice pattern. If cobalt is present at all, this results in a strained-epitaxy-like pattern (though we emphasize that this is a qualitative description of the pattern and not a hypothesis as to the structure) and/or strong higher order spots, and usually both. Indium and tin very often create disorder, whether they are intercalated first or second. Fe and Ni behave very similarly as first intercalants, with the structure determined by the second intercalant. As second intercalants, Fe and Ni are not particularly similar, which indicates a difference between adding mobile magnetic point defects to an existing intercalated structure and adding new intercalated material to a structure that already has a high density of mobile magnetic point defects. Indium has a weak tendency to make 1D superlattices with ordering reminiscent of In_2Se_3 superlattice diffraction patterns,[19] but this tendency is easily overpowered by preferred structures imposed by other elements as well as indium's apparent general tendency to yield disordered structures.

Each metal atom likely prefers specific interstitial sites in the van der Waals gap within the host Bi_2Se_3 lattice that lead to the formation of superlattice diffraction patterns. In the case of intercalation of multiple species, competition for these interstitial sites as well as interactions between the species create complex driving forces that evidently can yield a wide variety of ordered and disordered structures. The fact that the structure depends on the order in which the intercalants are introduced also indicates that at least some of these structures are metastable. Thus, controlling the processing conditions, including the order in which metals are intercalated can achieve frozen-in metastable structures that are otherwise unachievable, in effect greatly expanding the range of structural states that can be reached, and by implication the range of material properties one can access.

Nanoribbon morphology and structure are not changed with intercalation of multiple zero-valent atoms (Supporting Information; Figure S2). The TEM image of the nanoribbon of Figure 1 is representative of the mophology after processing. Intercalation occurs at such low temperatures so as not to disturb or destroy nanoribbons with processing.

DOI: 10.1021/jacs.5b00666
J. Am. Chem. Soc. 2015, 137, 5431−5437

X-ray Diffraction Superlattice Patterns. Superlattice patterns can also be observed in the X-ray diffraction (XRD) of these alloy-intercalated Bi_2Se_3 nanoribbons. Figure 3 shows

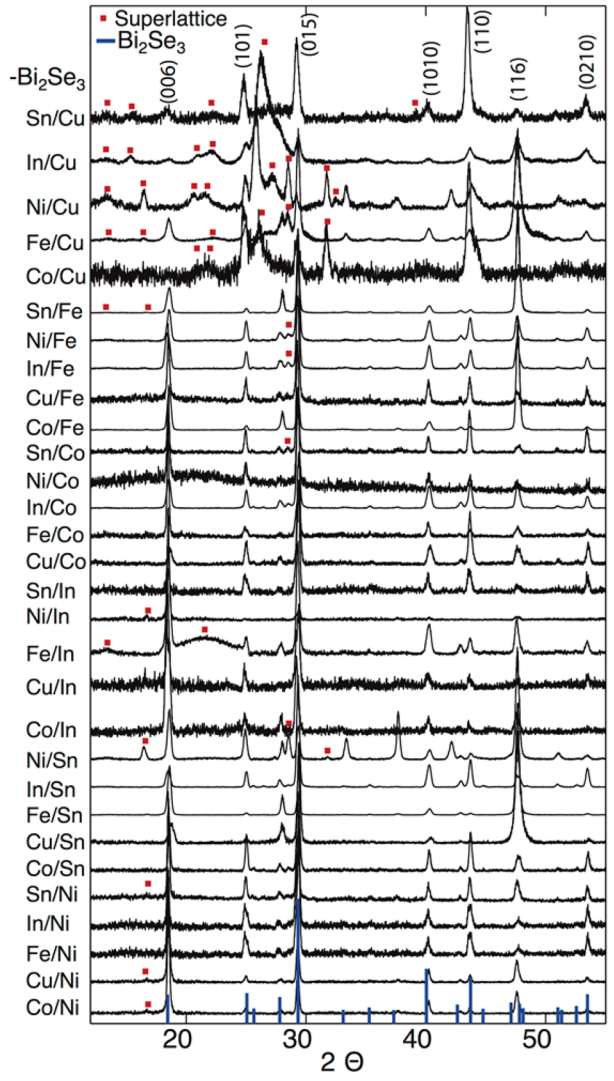

Figure 3. XRD of multi-element intercalated Bi_2Se_3 nanoribbons. Superlattice spots in the diffraction patterns are indicated by red dots.

the XRD of dual intercalated Bi_2Se_3 nanoribbons as indicated on the *y*-axis. Superlattice diffraction peaks are labeled with red stars. Peaks correspond to those observed in the electron diffraction patterns. It is interesting to note that intercalation of copper second leads to a series of strong superlattice peaks and a striking shift and intensity decrease of the (006) peak. Intercalation of copper results in very high densities of intercalant, up to 44 atomic percent in these studies even with the presence of other zero-valent species already in the nanoribbons. Copper may sit in interstitial sites or as a bilayer in the van der Waals gap which could result in stacking order changes and a decrease in intensity of associated host peaks such as the (006).[10] Lattice constants were determined through a Rietveld refinement of the Bi_2Se_3 host using Maud,[16] while intercalant concentrations were determined through TEM-EDX, averaging 3−5 nanoribbons for each measurement (Table 1). In nearly all multiple intercalations (Co/Sn being a counterexample), the *c* lattice constant increases with intercalation of multiple elements, which is consistent with expansion of the van der Waals gap as atoms intercalate. The contraction in the *c* lattice parameter found with Co/Sn is not completely unusual. In intercalation of ionic species both a lattice expansion or contraction is observed and is attributed to a wide range of factors including the size of the intercalant, the electrostatic interactions of the guest and host, and associated distortions of the host with guest uptake.[3,20] The *a* lattice constant, representing in-plane expansion, increases in nearly all cases as well (Cu/Sn being an exception). With the exception of Cu/Co, the expansion of the host lattice is significantly higher than single element intercalation nearly regardless of intercalant concentration.[11] The table does not show a clear systematic dependence of lattice expansion on either intercalant concentration or intercalant species for multiple intercalation. This is likely because of the complexity of the host + guest + guest system along with interatomic interactions between each intercalated species and the associated variety of resulting structures.

Optical Properties. Raman scattering of Bi_2Se_3 nanoribbons (Figure 4a) shows three Raman active modes including an

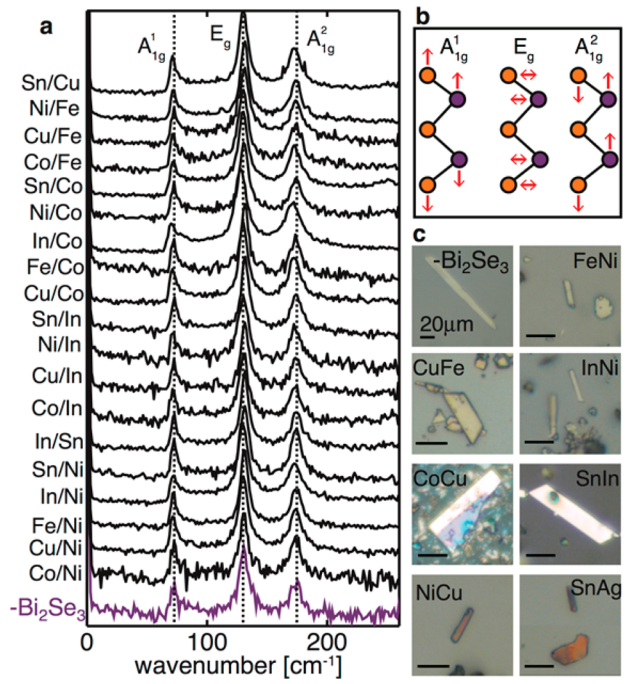

Figure 4. (a) Raman scattering spectra of multi-element intercalated Bi_2Se_3 nanoribbons show no shift of the phonon modes and no new peaks indirectly revealing minimal to no interaction of the guest and the host and no new modes, indirectly affirming the zero-valent metal character of the intercalant. (b) Raman active vibrational modes. (c) Optical images of large intercalated nanoribbons reveal color and/or reflectivity changes. Scale bars = 20 μm.

E_g mode (~130 cm^{-1}) and two A_{1g} modes (~70 and ~175 cm^{-1}). The E_g phonon mode corresponds to in-plane bond vibrations perpendicular to the *c*-axis; the A_{1g} modes correspond to the out of plane modes parallel to the *c*-axis (Figure 4b).[21] Nanoribbons intercalated with zero-valent metals show no shift of their out-of-plane Raman active phonon modes. This indirectly indicates that there is no bonding interaction between the zero-valent metal within the gap and the host. Bonding between the host and the guest should soften or stiffen the phonons resulting in a noticeable shift or broadening of peaks. The in-plane E_g mode shows little

DOI: 10.1021/jacs.5b00666
J. Am. Chem. Soc. 2015, 137, 5431−5437

to no shift as well within ±0.5 cm^{-1}. Since there is a change of the *a* lattice constant with intercalation, we expect some minor shift of this Raman mode. The exception is In/Co-intercalated Bi_2Se_3 which has a shift of the E_g phonon mode to 127.8 cm^{-1}. In/Co-intercalated Bi_2Se_3 also shows a Bragg signature of a planar incommensurate charge density wave, which may affect the optical phonon modes (Figure 1e). The intercalants do not introduce any apparent new Raman peaks. Since metals and alloys have no Raman active modes, as they are infinitely polarizable, this indirectly indicates that the metal intercalated into the nanoribbons retains a zero-valent character.

Recently, it was shown that intercalation of zero-valent copper into solvothermally grown, thin Bi_2Se_3 nanoplates can yield striking enhancement in both transmission and the conduction of the nanoplates.[22] Intercalation of multiple zero-valent metals may offer an even wider tunability in material optical properties. With intercalation of multiple zero-valent metals, not all but some of the nanoribbons undergo alteration in their optical appearance. Figure 4c shows a selection of optical images of Bi_2Se_3 nanoribbons intercalated with two metals. Though most ribbons (for example: Fe/Ni, Cu/Fe, In/Ni) show no change, nanoribbons intercalated with Co/Cu and Sn/In are strikingly reflective. Nanoribbons intercalated with Ni/Cu and Sn/Ag tend to have a more colored hue similar to nanoribbons intercalated with just zero-valent copper.[10] Further investigation into the optical properties of these various combinations may be worthwhile.

Oxidation State of Zero-Valent Alloy Intercalants. We use electron energy loss spectroscopy (EELS) to determine the oxidation state of the intercalant based on the near-edge fine structure, specifically through the L_3/L_2 peak height ratio and spectral shape.[11,12,23] With a single intercalated species in Bi_2Se_3, EELS shows that the intercalant remains zero-valent.[10,11] Figure 5a–c shows the EELS L_{23}-edge fine structure of Co/Ni, Cu/Ni, and Fe/Ni intercalated Bi_2Se_3 nanoribbons, respectively. Control spectra of common oxidation states of Ni, Fe, Cu, and Co are plotted with each spectrum.[11,23–28] Blue indicates a zero-valent reference, and red indicates the fine structure of an ionic element. Green is iron oxide (Fe_3O_4), in which Fe appears in both 2+ and 3+ oxidation states. For most cases, the EELS fine structure indicates that the intercalated element remains zero-valent, but there are some possible exceptions. Ni in the Cu/Ni case (Figure 5b) exhibits a very low signal-to-background ratio so that, after background subtraction, the measurement appears to marginally favor the 2+ oxidation state, but the noise level does not support a clear conclusion. In the Fe/Ni case (Figure 5c), the L_3/L_2 peak ratio clearly favors the +2 oxidation state, but the Fe^{2+} reference spectrum shows a very rapid rise after the L_2 peak that is not present in our measurements, so the assignment of the +2 state is uncertain. Such post-edge features can arise from sample thickness effects, which are expected since all of the samples are ~100 nm or more in thickness. However, this measurement suggests a surprising possibility: That the Fe enters the material in a +0 oxidation state but is oxidized later during the intercalation of the Ni^0 possibly influenced by magnetic interactions.

4. CONCLUSION

This work demonstrates that it is possible to intercalate multiple, zero-valent species into Bi_2Se_3 nanoribbons. Intercalants exhibit a variety of ordered and disordered structures (including superlattices and charge density waves) depending both on the intercalant species and the order in which they are introduced. For the most part, intercalants remain zero-valent. Given the general success of zero-valent intercalation into a host of layered and 2D materials, we believe that this method is general. This can be used to achieve a wide variety of new materials with unique optical and electronic properties previously inaccessible.

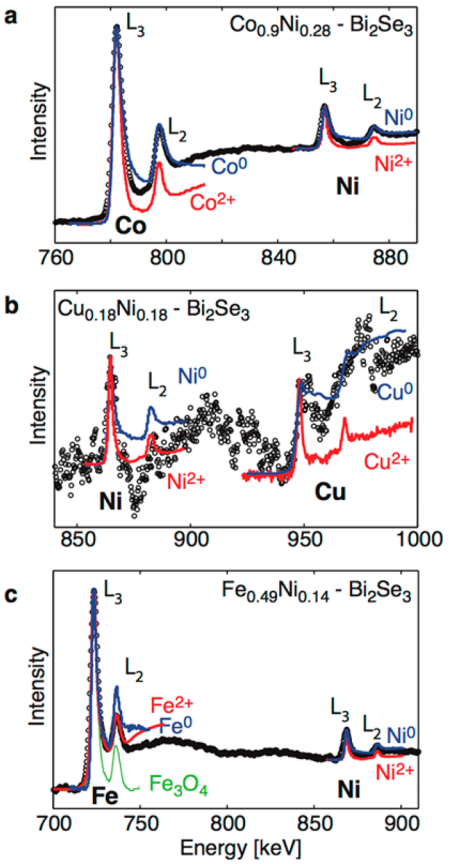

Figure 5. Background-subtracted EELS spectra of (a) Co/Ni, (b) Cu/Ni, and (c) Fe/Ni intercalated Bi_2Se_3 nanoribbons plotted with reference spectra[10,11,26–28] reveal oxidation state information on the intercalants by the ratio of the L_3 to L_2 peak heights.

■ ASSOCIATED CONTENT

Supporting Information

Additional STEM-EDX and TEM images, X-ray photoelectron spectroscopy data, reaction studies, and EDX spectra are supplied. This material is available free of charge via the Internet at http://pubs.acs.org.

■ AUTHOR INFORMATION

Corresponding Author

*koski@brown.edu

Notes

The authors declare no competing financial interest.

■ ACKNOWLEDGMENTS

K.J.K. gratefully acknowledges support through Brown University startup funds and the National Science Foundation (NSF DMR-1452523). F.R.C. was supported through the NASA RI space grant consortium.

DOI: 10.1021/jacs.5b00666
J. Am. Chem. Soc. 2015, 137, 5431–5437

REFERENCES

(1) *Progress in Intercalation Research*; Müller-Warmuth, W., Schöllhorn, R., Eds.; Kluwer: Dordrecht, The Netherlands, 1994.
(2) *Intercalation in Layered Materials*, NATO ASI Series, Subseries B, Physics; Dresselhaus, M. S., Ed.; Plenum Press: New York, 1987; Vol. *148*.
(3) *Intercalated Layered Materials*; Levy, F., Ed.; Reidel: Dordrecht, The Netherlands, 1979.
(4) Bruce, P. G.; Krok, F.; Lightfoot, P.; Nowinski, J. L.; Gibson, V. C. *Solid State Ionics* **1992**, *53*−*56*, 351.
(5) Huang, C. C.; Jang, G. W.; Chang, K. C.; Hung, W. I.; Yeh, J. M. *Polym. Int.* **2008**, *57*, 605.
(6) Cho, J. H.; Aykol, M.; Kim, S.; Ha, J. H.; Wolverton, C.; Chung, K. Y.; Kim, K. B.; Cho, B. W. *J. Am. Chem. Soc.* **2014**, *136*, 16116.
(7) Santhanam, R.; Noel, M. *J. Power Sources* **1995**, *56*, 101.
(8) Santhanam, R.; Noel, M. *J. Power Sources* **1998**, *76*, 147.
(9) Shirpour, M.; Cabana, J.; Doeff, M. *Energy Environ. Sci.* **2013**, *6*, 2538.
(10) Koski, K. J.; Cha, J. J.; Reed, B. W.; Wessells, C. D.; Kong, D.; Cui, Y. *J. Am. Chem. Soc.* **2012**, *134*, 7584.
(11) Koski, K. J.; Wessells, C. D.; Reed, B. W.; Cha, J. J.; Kong, D.; Cui, Y. *J. Am. Chem. Soc.* **2012**, *134*, 13773.
(12) Motter, J.; Koski, K. J.; Cui, Y. *Chem. Mater.* **2014**, *26*, 2313.
(13) Zhang, H.; Liu, C. X.; Qi, X. L.; Dai, X.; Fang, Z.; Zhang, S. C. *Nat. Phys.* **2009**, *5*, 438.
(14) Kong, D.; Randel, J. C.; Peng, H. L.; Cha, J. J.; Meister, S.; Lai, K.; Chen, Y.; Shen, Z.-X.; Manoharan, H. C.; Cui, Y. *Nano Lett.* **2010**, *10*, 329.
(15) Kong, D.; Cha, J. J.; Lai, K.; Peng, H.; Analytis, J. G.; Meister, S.; Chen, Y.; Zhang, H.-J.; Fisher, I. R.; Shen, Z.-X.; Cui, Y. *ACS Nano* **2011**, *5*, 4698.
(16) *Maud - Materials Analysis Using Diffraction*; University of Trento: Trento, Italy; http://www.ing.unitn.it/~maud/.
(17) Wilson, J. A.; Di Salvo, F. J.; Mahajan, S. *Adv. Phys.* **1975**, *24*, 117.
(18) Gschneidner, K.; Russell, A.; Pecharsky, A.; Morris, J.; Zhang, Z. H.; Lograsso, T.; Hsu, D.; Lo, C. H. C.; Ye, Y. Y.; Slager, A.; Kesse, D. *Nat. Mater.* **2003**, *2*, 587.
(19) Ye, J.; Soeda, S.; Nakamura, Y.; Nittono, O. *Jpn. J. Appl. Phys.* **1998**, *37*, 4264.
(20) Prasad, S. S. In *Handbook of Solid State Batteries and Capacitors*; Munshi, M. Z. A., Ed.; World Scientific: Singapore, 1995; 467.
(21) Zhang, J.; Peng, Z.; Soni, A.; Zhao, Y.; Xiong, Y.; Peng, B.; Wang, J.; Dresselhaus, M. S.; Xiong, Q. *Nano Lett.* **2011**, *11*, 2407.
(22) Yao, J.; Koski, K. J.; Luo, W.; Cha, J. J.; Hu, L.; Kong, D.; Narasimhan, V. K.; Huo, K.; Cui, Y. *Nat. Commun.* **2014**, *5*, 5670.
(23) Leapman, R. D.; Grunes, L. A.; Fejes, P. L. *Phys. Rev. B* **1982**, *26*, 614.
(24) Wang, Z. L.; Yin, J. S.; Jiang, Y. D. *Micron* **2000**, *31*, 571.
(25) Pearson, D. H.; Ahn, C. C.; Fultz, B. *Phys. Rev. B* **1993**, *47*, 8471.
(26) Vodungbo, B.; Zheng, Y.; Marangolo, M.; Demaille, D.; Varalda. *J. Phys.: Condens. Matter* **2007**, *19*, 116205.
(27) Quintana, C.; Menéndez, J. L.; Huttel, Y.; Lancin, M.; Navarro, E.; Cebollada, A. *Thin Solid Films* **2003**, *434*, 228.
(28) Cave, L.; Al, T.; Loomer, D.; Cogswell, S.; Weaver, L. *Micron* **2006**, *37*, 301.

DOI: 10.1021/jacs.5b00666
J. Am. Chem. Soc. 2015, 137, 5431−5437